Ultrasonics Sonochemistry 86 (2022) 106024

Contents lists available at ScienceDirect

Ultrasonics Sonochemistry

journal homepage: www.elsevier.com/locate/ultson

Ultrasound-assisted fabrication of Ti_3C_2Tx MXene toward enhanced energy storage performance

Xinyue Zhang, Wu Zhang *, Haitao Zhao

School of Materials Science and Engineering, Shenyang Ligong University, Shenyang, Liaoning 110159, PR China

ARTICLE INFO

Keywords:
Ti_3C_2Tx MXene
Ultrasound
Energy Storage performance

ABSTRACT

Ti_3C_2Tx MXenes are normally fabricated by removal of main group element from the corresponding transition metal carbides, and they have been actively studied due to their superior energy storage performance. However, the low efficiency in removal of main group element (named as chemical etching) has significantly limited the application of MXene or MXene-related materials. Herein, we demonstrated an ultrasound-assisted approach to synthesize Ti_3C_2Tx MXene material by using Ti_3AlC_2 as the precursor. The experimental results indicate that the efficiency of chemical etching of Ti_3AlC_2 was dramatically promoted by ultrasound. The etching time was greatly shortened to 8 h while typically 24 h is sufficient in dilute hydrofluoric acid. Particularly, the high etching efficiency was achieved by using 2% hydrofluoric acid under the aid of ultrasound, which is lower in concentration than those reported in the previous literature. The specific capacitance of the 8 h sonicated sample is 155F/g, which is much higher than that of the un-sonicated sample prepared under the same experimental conditions. Additionally, the specific capacitance retention of the prepared 8 h sonicated sample was 97.5% after 20,000 cycles of charging/discharging, exhibiting an outstanding energy storage stability compared with the materials reported in previous literatures. It was proposed that removal of AlF_3 from the surface of the etched particles was significantly promoted and the hydrogen bonds between the terminations of two different adjacent layers were broken by the acoustic cavitation effect of ultrasound.

1. Introduction

MXenes are normally fabricated by removal of main group element from the corresponding transition metal carbides. MXene and MXene-based materials find their application in a variety of fields, including energy storage, catalysis, sensors, nanogenerator, desalination, and microwave shielding [1,2]. For example, self-assembled MXene nanostructures possess superior catalytic performances for water treatment and hydrogen production [3,4,5]. MXene or MXene-based materials are commonly prepared from their corresponding MAX precursors, which exhibit 3D crystal structure but consist of the bonding and stacking of 2D layered structures. In the structure of MAX, the "M" represents early transition metals. e.g., V, Ti and Mo. "A" consists of main group elements, typically those elements from groups 13 and 14, such as Al, Si, Zn, and Ga. Regarding the "X" element in the MAX structure, a prime example is C [6]. As an alternative, N is also considered as a suitable candidate for "X" component. A characteristic of MAX materials is the octahedral layered structure, which planarly extends by an edge-sharing configuration and thereby forms an "M−X" layer structure. The "A" atoms are located intermediately between two different "M−X" layers [6]. Consequently, rearrangement of the MAX to prepare its corresponding MXene structures could be achieved by selective removal of "A" atoms while keeping the MX layers in the original structure, which is known as etching of MAX precursors. The resultants of etching of MAX materials normally exhibit accordion-like structures. A more appealing characteristic of the as-prepared MXenes is that the stacked accordion-like MXenes could be delaminated into monolayered or few-layer nanosheets, which shows superior properties, such as high specific surface area, good hydrophilicity, and rich surface chemistry, compared with their original accordion-like counterparts.

To date, various methods and etchants have been developed. Among the abundant etching etchants, hydrofluoric acid (HF) is the first and mostly reported etchant to obtain MXenes from their corresponding MAX precursors. Naguib et al. [7] employed 50% HF as the etchant to remove Al components in the MAX phase, and accordion-like Ti_3C_2Tx MXene powder with van der Waals force and hydrogen bonds between each layer was obtained, the resulting Ti_3C_2Tx MXene powder was consistent with the corresponding Ti_3AlC_2 MAX phase in stoichiometry

* Corresponding author.
E-mail address: neusmmzhangwu@163.com (W. Zhang).

https://doi.org/10.1016/j.ultsonch.2022.106024
Received 5 February 2022; Received in revised form 29 April 2022; Accepted 30 April 2022
Available online 5 May 2022

and crystal structure, excepting that the Al atomic layer was removed. Although the feasibility of high concentration hydrofluoric acid for MAX phase etching has been experimentally proved, the harsh etching reactions and the dissolved oxygen gas in aqueous etchants induce extra structural defects to the resulting MXenes and promote their degradation into TiO_2. Fluorine-containing salts, such as KHF_2, $NaHF_2$, and NH_4HF_2, have been developed to perform the etching of MAXs, the etching time is usually more than 24 h, which leads to a low efficiency for preparation of MXene [8]. Recently, electrochemical etching approaches emerged to get desired materials with high efficiency [9,10]. A prime example is that $CuCl_2$ molten salt has been employed to etch MAX powders [9]. Apparently, a high temperature (approximately 750 °C is needed in the etching process, which sets an obstacle to the practical production and application of the molten salt method. Aqueous solutions have also been considered as suitable baths for electrochemical etching of MAX precursors, it was found that a significant anodic effect and the resulting emission of toxic gas make it an undesirable route for etching of the MAX phase.

Ultrasound has been widely employed in extraction [11], food processing [12], emulsification [13], and other fields. Additionally, it is currently gaining popularity as a promising technique for material synthesis due to its green, innovative, and cost-effective characteristics. Various materials such as nanostructured materials [14], conducting polymers [15], and photocatalysts [16], have been successfully prepared by ultrasound-assisted approaches. Introduction of ultrasound can provide extra energy to the as-used solution, allowing better mass transfer than those for the un-sonicated solutions in mixing, drying, and extraction processes. In this regard, ultrasound is a suitable candidate for improving the efficiency of etching Ti_3AlC_2 during preparation of MXenes.

As mentioned above, MXenes have attracted great attention as next-generation capacitive energy-storage materials. In this regard, although MXenes show promising application prospects in energy storage, the practical electrochemical performance of few- and mono-layered MXenes falls short of expectations, and no commercialized MXenes are available to date. This results from the blocking effect of surface anion and excessive accumulation of layers. As an alternative, accordion-like MXenes, which are physically more stable and possess higher cycling stability than the few- and mono-layered ones, are attracting more and more attention as promising energy storage materials.

Inspired by the advantage of MXenes in the field of energy storage, Ti_3C_2Tx was synthesized by using Ti_3AlC_2 in the present work. As described previously, the most challenging issues for preparation of MXenes can be summarized as: (1) low etching efficiency while chemical reagents were used except for high concentration hydrofluoric acid; (2) When concentrated hydrofluoric acid is used as the etchant, the harsh reactions induce extra structural defects; (3) The high temperature or significant anodic effects limits the application of electrochemical approaches for etching of MAX phase. To address the above challenges, dilute hydrofluoric acid (2 wt%) was used as the etchant to ease the experimental conditions and prevent the formation of TiO_2, of particular to this work is the introduction of ultrasound, which is a highly energy-efficient method for material synthesis, thereby achieving efficient etching of Ti_3AlC_2 precursor.

2. Experimentation

2.1. Materials and instrumentation

In the present work, All the chemical reagents were purchased from Shanghai Macklin Biochemical Co., Ltd and were used without further purification. Powdery Ti_3AlC_2 (purity: 98 %, average particle size: 74 μm) and hydrofluoric acid were used as a precursor and the etchant, respectively. 1 M H_2SO_4 solution serves as the electrolyte to test the electrochemical properties of the synthesized materials. Deionized water (DI water) was used throughout the experiments for any washing purpose or preparation of desired solutions. Acetylene black, polyvinylidene fluoride (PVDF), as well as N-methylpyrrolidone (NMP), were used to prepare the electrode. Carbon paper (purchased from Toray Industries, Inc. Japan.) was used as the collector to prepare the working electrode.

X-ray diffractometer (XRD, MPDDY2094, Netherlands) with Cu Ka radiation (λ = 0.15406 nm) was operated at a scan range of 5°~90° to study phase composition of the as-prepared samples. Scanning electron microscope (SEM, Tescan Vega II, Czech Republic), equipped with Energy Dispersive Spectrometer (iXRF Systems, 550i) was used to study the morphology of the samples. XPS experiments were carried out using an ESCALAB 250Xi (Thermo Fischer) X-ray photoelectron spectrometer with a basic chamber pressure of $4 \times l0^{-9}$ mbar. Al anode was used as the X-ray source (x-ray radiation of 1486.6 eV) in the XPS characterization with a working voltage at 14.6 kV. An ICP-OES (Thermo Scientific, icap pro) was used to perform analyzing of the Al content in the samples.

All the electrochemical tests, including cyclic voltammetry (CV), galvanostatic charge/discharge (GCD) measurements, and electrochemical impedance spectroscopy (EIS), were performed using a CHI 760E (purchased from Shanghai CH Instrument Co., Ltd) electrochemical workstation. A sonicator (Model: KQ 2200DE, purchased from Kunshan Ultrasonic Instruments, Co. Ltd.) was employed to generate ultrasound during the etching experiments. A 50 ml Teflon autoclave with a 2 mm diameter open pore on the gap to emit the generated gas served as the container to perform etching experiments. A centrifuge (Model: TG16-WS, Shanghai Luxiang Centrifuge Instrument Co., Ltd) was used for centrifugal experiments.

2.2. Experimental procedure

2.2.1. Preparation of the Ti_3C_2Tx MXene powders

According to the information from previous literatures, all the etching experiments were performed at 50℃ throughout the work. Briefly, 2 g Ti_3AlC_2 was added at a rate of 0.2 g/min into 2 wt% hydrofluoric acid solution in 10 mins to avoid intense boiling. The solution was heated in a water bath in the sonicator. The sonication assisted wet-chemical etching of the Ti_3AlC_2 powders as the temperature was increased to 50℃. The acquired slurry was repeatedly centrifuged for 15 cycles at 5000 rpm/min for 3mins for each cycle of operation until the pH of the supernatant was close to 6.5. Subsequently, the mixture was filtered by using a vacuum suction pump. The filter cake was dried in the vacuum oven at 50℃ for 12 h. The hydrofluoric acid etching treatment can be represented by: [17].

$$Ti_3AlC_2 + 3HF = Ti_3C_2 + AlF_3 + 3/2H_2 \quad (1)$$

$$Ti_3C_2 + 2H_2O = Ti_3C_2(OH)_2 + H_2 \quad (2)$$

$$Ti_3C_2 + 2HF = Ti_3C_2F_2 + H_2 \quad (3)$$

2.2.2. Fabrication of the electrode

Regarding fabrication of the electrode, the as-prepared Ti_3C_2Tx MXene powders were mixed with acetylene black and polyvinylidene fluoride (PVDF) at a mass ratio of 8:1:1, among which the acetylene black and PVDF serve as the conductor and binder, respectively. Typically, 10 mg acetylene black and 10 mg PVDF were consecutively added into 80 mg MXene powder, the mixture was then mixed with 0.5 ml NMP in a 20 ml Teflon container and then was magnetically stirred for 3 h at room temperature to achieve sufficient mixing of the slurry. Subsequently, the acquired slurry was then uniformly coated on a 1 × 2 cm carbon paper with an active area of 1 × 1 cm. The newly prepared electrode was dried in a vacuum oven for 12 h to perform electrochemical tests.

2.2.3. Electrochemical tests

Prior to the electrochemical tests, the prepared electrodes were soaked in the electrolyte for 12 h to make the electrolyte fully adsorbed on the active materials. Cyclic voltammetric (CV) experiments were performed at a scan range of 10 ~ 100 mV/s with an interval of 20 mV/s. Galvanostatic charge–discharge (GCD) tests were performed within the selected potential range of CV from 1A/g to 5A/g. Electrochemical impedance spectroscopy (EIS) measurements were conducted from 100 kHz to 0.01 Hz with an amplitude of 5 mV starting from open circuit potential (OCP). Galvanostatic cycling experiments were performed at a current density of 1 A/g. The specific capacitance can be calculated by using the acquired CV and GCD curves, the corresponding equations are shown as follows [18]:

$$C = \frac{\int IdU}{mv\Delta U} \tag{1}$$

$$C = \frac{I\Delta t}{m\Delta U} \tag{2}$$

where C (F/g) represents specific capacitance, F/g; m stands for the mass of active material in the working electrode, (g); v is the scan rate of CV in unit mV/s; ΔU (V) is the potential window in the CV or GCD curve in unit V; I is the generated current, A; Δt is the discharge time, s.

3. Results and discussion

3.1. Material characterization

3.1.1. XRD patterns of the samples

Fig. 1(a) depicts the XRD patterns of the pristine $Ti_3Al_2C_2$ powder and the etched samples in absence and in presence of sonication. It is vividly shown that the etched samples hold the same crystal structure as the corresponding $Ti_3Al_2C_2$. Naguib and coworkers [19] etched the $Ti_3Al_2C_2$ by using 50% hydrofluoric acid, it was reported that the stoichiometry and crystal structure of the resultant Ti_3C_2Tx powder was consistent with the pristine Ti_3AlC_2 MAX phase except for the Al atomic layer, which is in good agreement with the results in the present work. As shown in Fig. 1(a), the characteristic (0 0 2) peaks of as-prepared MXene shifted from 9.6° in the Ti_3AlC_2 powder to a lower 2θ angle of 9.5° after 8 h of etching treatment in absence of ultrasound, and it further shifts to 9.4° when the ultrasound is present. According to the Bragg's law [20], this is an indication of an increase in interlayer spacing due to the removal of Al and introduction of surface terminations (represented as Tx) in Ti_3C_2Tx (e.g., -F, -O, –OH) in the wet-chemical etching of Ti_3AlC_2. Additionally, the intensity of decrease with proceeding of etching, and the peaks of the samples with sonication was further decreased compared with that of the non-sonicated sample, which demonstrates that the etching process was promoted by sonication. Fig. 1 (b) shows the XRD patterns of the samples with different timescale of sonication (from 1 h to 8 h). The peaks of (0 0 2) shifted to the lower angle as the time increased from 1 h to 8 h and, the width of (0 0 2) peak become larger with the increasing of sonication time, this indicates a gradually enlarged interlayer spacing of (0 0 2) plane. Notably, the peak at ca. 20° in Fig. 1(a) and (b), corresponding to (0 0 4) plane of the Ti_3AlC_2 structure, lose intensity in the 8 h-sonicated sample, which is ascribed to the successful removal of Al for the pristine Ti_3AlC_2.

It was reported that the characteristic peaks at around 39°completely disappeared when the mono-or few-layered MXene was synthesized by using 50 wt% hydrofluoric acid at 50 °C for 2 h, which is not in agreement with the results in the present work[21]. Additionally, it is noteworthy that all the etched (sonicated and un-sonicated) samples show pronounced diffraction peaks throughout the whole scan range of XRD in Fig. 1, which is a distinct difference from those of few- or mono-layered MXenes [21]. The above findings suggest that the no appreciable few- or mono-layered MXenes are generated throughout the etching treatment in the present work, and this will be further discussed in the present work.

3.1.2. SEM observation

SEM images of the samples in absence of and in presence of ultrasound are shown in Fig. 2(a) to (f). It is observed that the etching trails emerged in the first hour of etching in presence of ultrasound. With the increasing of etching time, more pronounced etching trails are observed. Typical accordion-like morphology is shown in Fig. 2(c) and (f), the sample with 8 h of sonication. Fig. 2(a) and (d) show the morphology of the etched sample for a treatment of 8 h in absence of ultrasound. Compared with the samples shown in Fig. 2(c) and (f), no well-defined etching trails are observed in the un-sonicated sample shown in Fig. 2 (a) and (d), indicating that the etching process is effectively promoted by the ultrasound. Additionally, the surface of the samples in absence of ultrasound is covered by nodular structures, likely the AlF_3 by-product according to Eqn. (1) in the present work, which prohibits an efficient etching of the Ti_3AlC_2. The 8 h sonicated sample was tested by elemental mapping; the results are shown in Fig. 2(g) to (j). Compared with the other three elements, only a small amount of Al components is detected in the 8 h sonicated sample. In addition, the distribution of F significantly differs from that of the Al element, indicating that AlF_3 is not present on the surface of the 8 h sonicated sample.

The variation of Al content based on the ICP-OES determination results are shown in Fig. 3, i.e., the removal rate of Al for the cases in

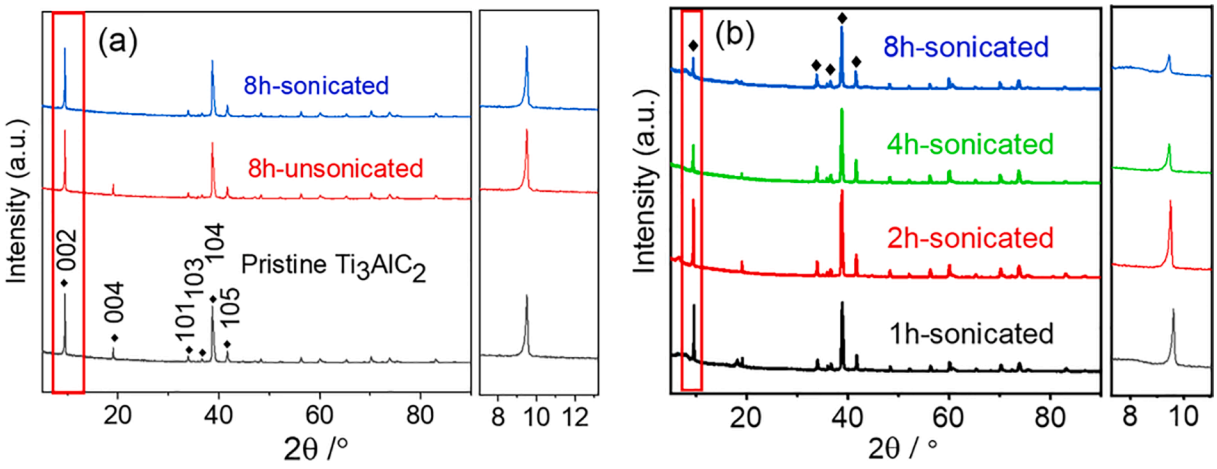

Fig. 1. (a): XRD patterns of the pristine Ti_3AlC_2 and the etched samples in presence of and in absence of ultrasound; (b): variation of XRD patterns with sonication time (from 1 h to 8 h).

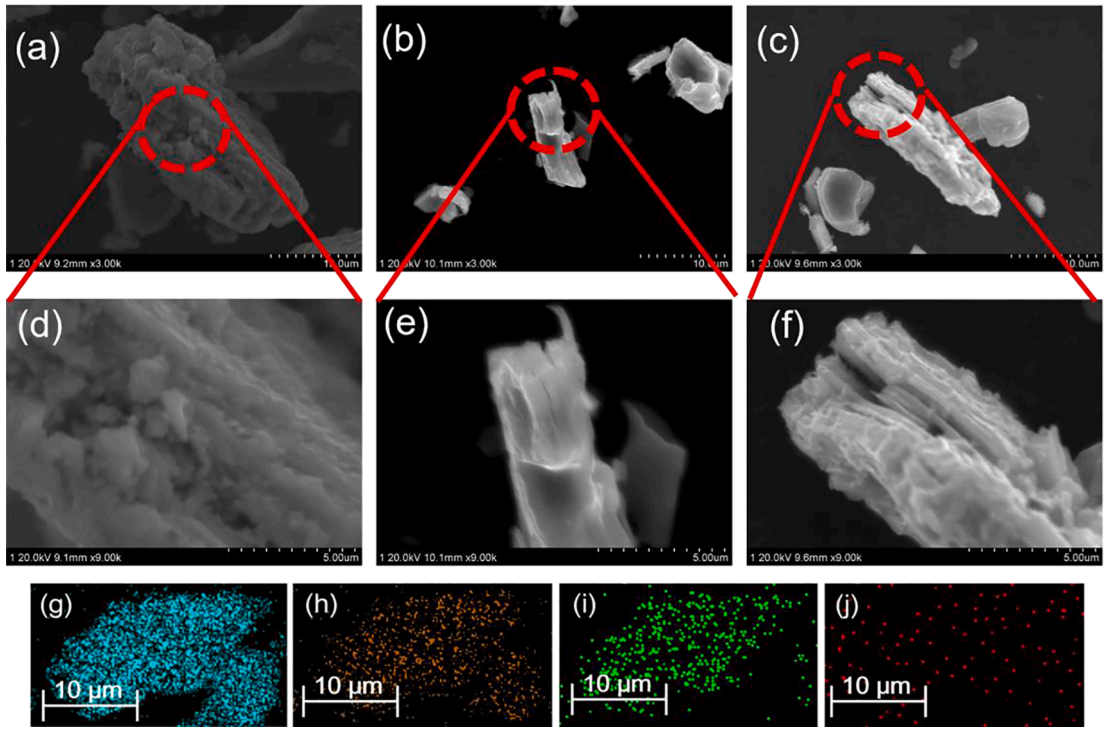

Fig. 2. SEM images of the samples in absence of and in presence of ultrasound (a and d: un-sonicated sample for 8 h etching; b and e: sonicated sample for 1 h etching; c and f: sonicated sample for 8 h etching; g to j: elemental mapping of Ti(g), C(h), F(i) and Al(j) in the 8 h etched sample in presence of ultrasound.

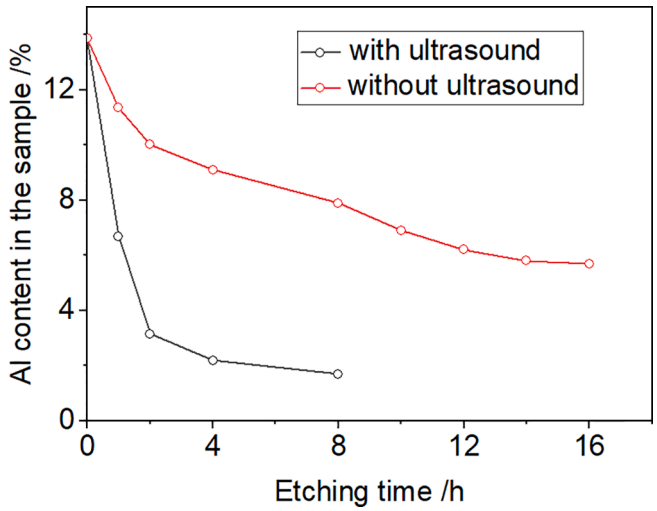

Fig. 3. Variation of Al content in the etched samples.

presence of and in absence of ultrasound. It is clearly shown that the removal rate of Al is much faster than that of the un-sonicated case.

In particular, only ca.3% Al is left in the Ti_3AlC_2 structure for the first two hours of etching in presence of ultrasound, while the corresponding value for the case of without ultrasound is 10.05%, indicating a much faster removal rate of Al for the ultrasound aided case than those of without ultrasound. Notably, the Al contents in the etched sample are close to a constant value (1.71% and 5.72% for the sonicated and un-sonicated cases, respectively) after the etching treatment. Alhabeb and coworkers have done some profound work on preparation of Ti_3C_2Tx MXenes [22]. They employed 5 wt% and 10 wt% fluohydric acid as the etchant to prepare accordion-like Ti_3C_2Tx MXenes, which were further delaminated into monolayered ones, the required etching time is 24 h and 18 h, respectively [22]. Mashtalir et al. [23] studied the kinetics of aluminum extraction from Ti_3AlC_2 in 50% hydrofluoric acid, it was found that at least 15 h were needed to complete removal of Al from Ti_3AlC_2. In-situ HF forming systems for Ti_3AlC_2, such as high concentration of LiF/HCl and NH_4HF_2, which inherently use HF as the active reagent for etching of Ti_3AlC_2, even showed lower efficiency in removal of Al than fluohydric acid. The etching efficiency has been significantly improved in the present work. Additionally, the lowest concentration of fluohydric acid to prepare Ti_3C_2Tx MXene is 5% to date, the concentration of fluohydric acid is further decreased to 2% in this study, while better performance of the products is achieved, thanks to the applied ultrasound.

3.1.3. XPS characterization

X-ray Photoelectron Spectroscopy (XPS) spectra of the prepared samples are shown in Fig. 4. Fig. 4(a) depicts the full spectra of sonicated samples with the sonication time of 1 h, 2 h, 4 h, and 8 h. In Fig. 4(a), the peak at 284.8 ev is the characteristic peak of C1s, and the four peaks at 33.04, 57.9, 453.9, and 560.1 ev correspond to Ti 3p, Ti 3 s, Ti 2p, and Ti 2 s. In addition to the Ti and C-related peaks, the characteristic peaks of F1s and O1s at 688.3 and 529.5 ev, which are absent from the pristine Ti_3AlC_2, are detected. Additionally, similar trails of the four XPS curves is observed. This suggests that the Ti_3AlC_2 precursor is continuously etched throughout the 8 h and oxidation of Ti and C in the precursor is present. To further confirm this information, high-resolution XPS spectra were conducted by using the 1 h and 8 h sonicated samples. The high-resolution C 1 s spectrum of 1 h exhibit the peaks at 284.8, 285.75, 287.72, and 288.54 eV, which belong to C–C, C-O, C = O, CF_3-C = O chemical bonds, respectively [24], and this demonstrates that the C element in the sample is continuously oxidized and fluoridized. Interestingly, the CF_3-C = O chemical bond transferred to C_6F_6 chemical bond [25], which corresponds to the peak at 289.42 eV in Fig. 4(c), and this is a strong indication for further fluoridized of the etched samples.

The behavior of fluoride is barely discussed in the previous literatures. Here the high-resolution F 1 s spectrum is conducted by using 1 h and 8 h sonicated samples. In the high-resolution F 1 s spectrum of 1 h sonicated sample (Fig. 4(d)), the peak corresponding to $(–CH_2\text{-}CF_2\text{-})_n$ at

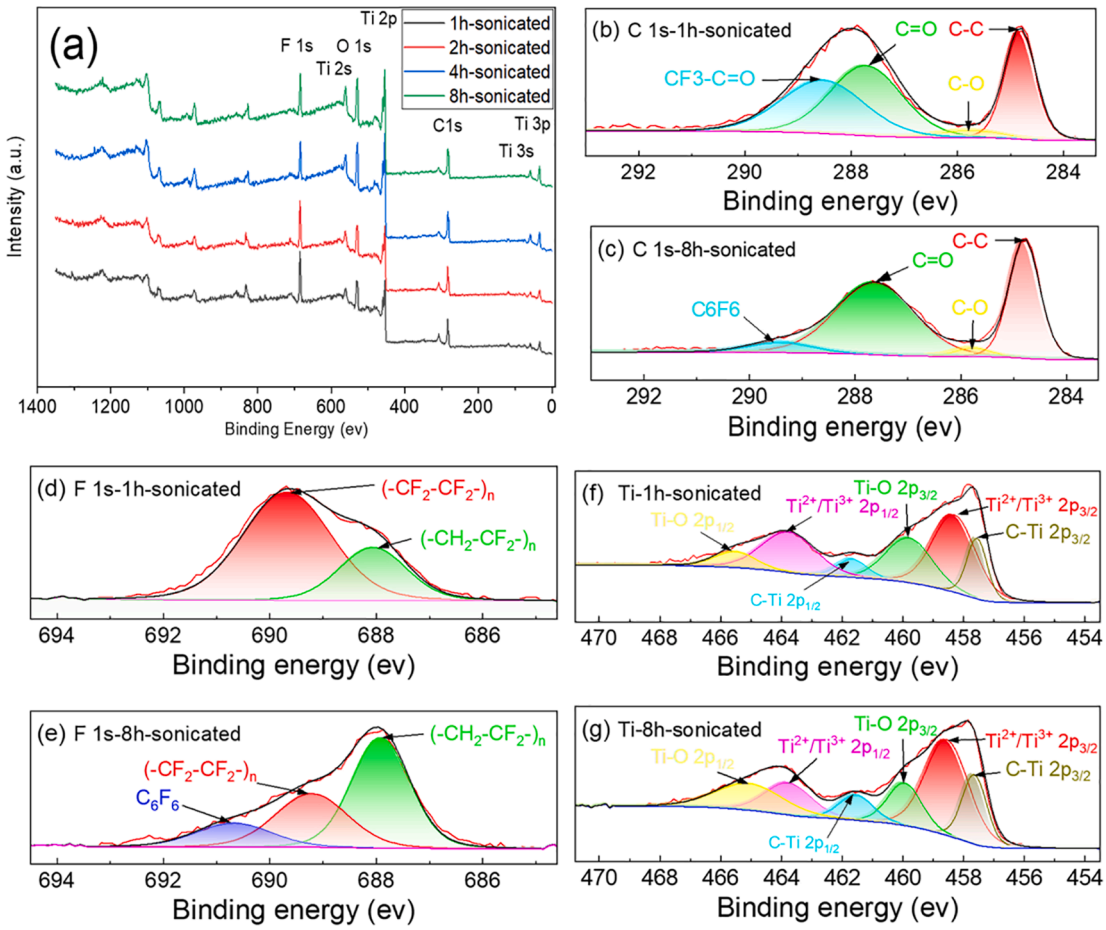

Fig. 4. (a) XPS survey of the samples with the sonication time of 1 h, 2 h, 4 h, and 8 h; (b) to (g): high-resolution spectrum of C 1 s(b) and (c), F 1 s(d) and (e), Ti (g) and (h) for the 1 h and 8 h sonicated samples.

689.68 ev is observed, indicating that the Al atoms are partially substituted by hydrogen and fluoride atoms. Another peak at 688.07 ev is observed, which is a characteristic of $(-CF_2-CF_2-)_n$ chemical bonds. i. e., the hydrogen atoms are removed and replaced by fluorine atoms in the precursor. With the proceeding of the etching, a new peak at 690.8 ev is detected, which is a diagnostic criterion of C_6F_6 group, indicating that the Ti atoms locating at the edge of the MAX phase are substituted by fluoride, which is not reported in the previous literature. The high-resolution Ti spectrum of 1 h and 8 h sonicated samples are presented in Fig. 4(f) and (g), six peaks with respectively similar binding energy are observed in both graphs, suggesting that the chemical and electronic environment of Ti atom are not altered with the timescale of etching. The peaks in Fig. 4(f) and (g) at 457.64, 458.55, 459.95, 461.54.1, 463.77 and 465.07 eV correspond to Ti-C $2p_{3/2}$, Ti^{2+}/Ti^{3+} $2p_{3/2}$, Ti-O $2p_{3/2}$, Ti-C $2p_{1/2}$, Ti^{2+}/Ti^{3+} $2p_{1/2}$ and Ti-O $2p_{1/2}$, respectively. The high-resolution Ti spectrum in Fig. 4(f) and (g) proves the oxidation of Ti atoms into TiO_2 in the precursor, which has been found in the previous literature. [26].

3.2. Electrochemical performance of the samples

Prior to testing the electrochemical performance of the samples, stability of the samples is an issue to be considered. To determine the stability of the samples, duplicate experiments were performed, no appreciable decomposition of the sample was found, i.e., the prepared samples are thermally and electrochemically stable under the tested conditions. To evaluate the electrochemical performance of the $Ti_3C_2T_x$ MXene, cyclic voltammetric (CV) experiments were performed in a three-electrode configuration. The performed potential range of CV was selected within the decomposing potential of the electrolyte. Fig. 5 depicts the CVs of different samples at different scan rates from 10 mV/s to 100 mV/s.

It is vividly shown that the electrochemical properties of sonicated samples improved significantly with increasing of the timescale of sonication. Regarding the CV of the sample in absence of ultrasound, no well-defined trails for typical behaviors of the energy storage materials were observed, and the specific capacitance of the 8 h un-sonicated sample (Fig. 5(a)) at 10 mV/s was calculated to be only 3.4F/g, while the corresponding specific capacitance for the sonicated sample (Fig. 5 (d)) with the same timescale of treatment is 155F/g, which is a significant improvement in specific capacitance compared with the un-sonicated sample. Wu et al. [20] synthesized organ-like $Ti_3C_2T_x$ MXene by using hydrofluoric acid for 24 h, they reported a specific capacitance of ca. 100F/g at the same scan rate (10 mV/s). Additionally, the specific capacitances of the sonicated samples are 4.3, 6.9, 100, and 155F/g with the sonication time of 1 h, 2 h, 4 h, and 8 h, which experimentally proves that prolonging of sonication time favors the electrochemical performance of the acquired MXenes. This is in good agreement with our SEM observation in the present work.

The capacitive behavior of the as-prepared 8 h etched samples with and without ultrasound was studied through galvanostatic charge–discharge (GCD) measurements in the range from 1A/g to 5 A/g (Fig. 6(a) and (b)). It is observed that the GCD curves of the sonicated sample show better symmetrical triangles than those of the un-sonicated sample. As expected by the results in CV tests, the sonicated sample with 8 h of treatment exhibits better capacitive behavior than the un-sonicated MXene, better reversibility of the electrochemical performance. The specific capacitances of the 8 h sonicated sample are 180,

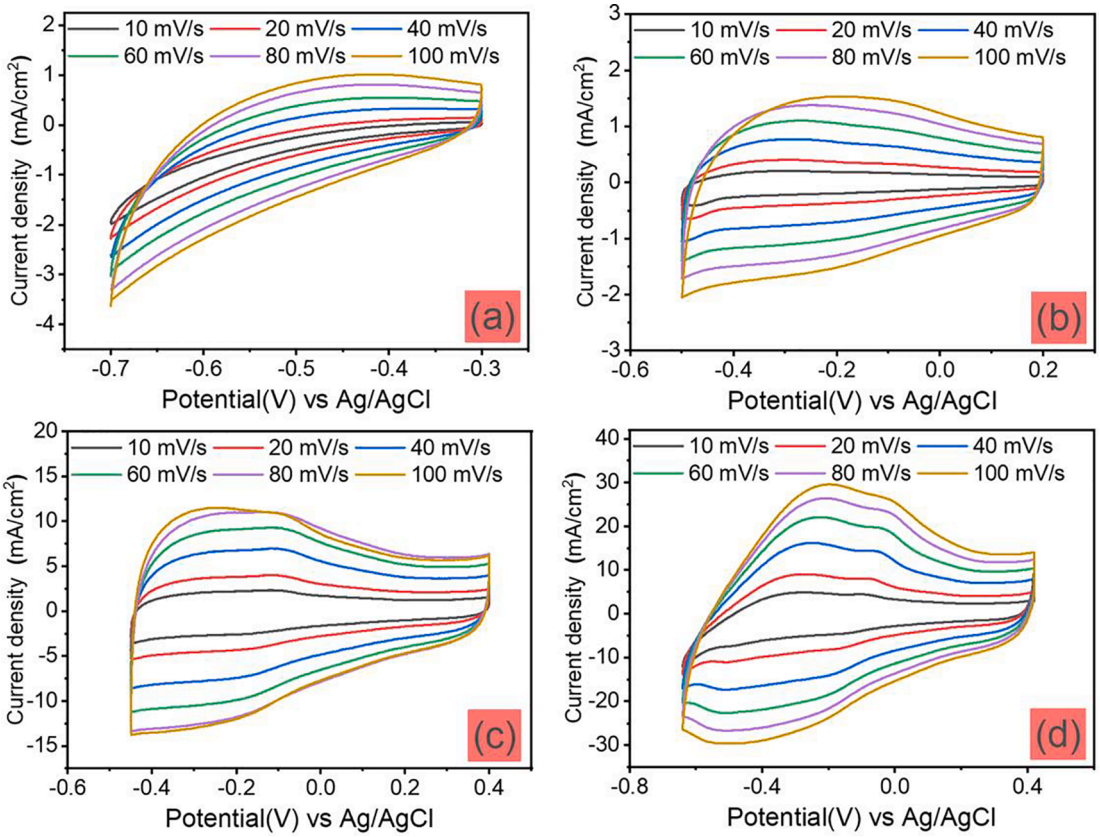

Fig. 5. Cyclic voltammograms (CV) of the prepared samples with scan rate from 10 to 100 mV/s; (a) 8 h-unsonicated; (b) 2 h-sonicated; (c): 4 h-sonicated; (d) 8 h-sonicated.

124.8, 111.8, 103.3, and 91F/g as the current density increase from 1 to 5 A/g. The GCD curve of the 8 h sonicated sample retains a superior rate capability of ca 50% at 5 A/g, indicating an outstanding quick charge–discharge performance of the electrode prepared by the 8 h sonicated sample. Electrochemical impedance spectroscopy (EIS) was further performed to study the charge transfer resistance (Rct) and ion transport in the tested electrode [27,28], Nyquist plots of all samples showed negligible semicircles and a relatively low Rct, suggesting that removal of Al did not significantly affect the electronic conductivity of Ti_3C_2Tx. In the low-frequency range, interpretation of Nyquist plots for all the four tested electrodes suggests a good ionic conductivity of the electrodes, i.e., at low frequencies, the slope of the plot for 8 h-unsonicated sample shows lower diffusion resistance compared to the sonicated samples. This is ascribed to the lower concentration of surface terminal groups caused by the AlF_3 byproduct, which is discussed in the SEM observation in the present work. The real axis intercept at high frequency corresponds to the uncompensated resistance of the bulk electrolyte solution (Rs), as observed in Fig. 6(d), here the Rs values for the sonicated samples are found to be smaller than that of the un-sonicated sample. Variation of specific capacitance with the scan rate of CV was listed in Table 1, it is shown that the specific capacitance decreases with the increase of scan rate for all the four samples, this could be assigned to the contribution of diffusion of ions in the electrolyte. At large scan rates, for example, 100 mV/s, the ions do not have enough time to diffuse into the surface of the active material, thereby decreasing the specific capacitance of the as-prepared MXenes.

Apart from specific capacitance, cycling stability is attractive merit of electrochemical capacitors, it is a key factor to determine the potential of the electrode material for practical applications. Herein, GCD experiments were performed for 20,000 cycles at 5 A/g to determine the cycling stability of the MXene, the results are shown in Fig. 7, inset of Fig. 7 shows the profile of the first and the last cycles of GCD curves. The capacitance retention of the electrode is 97.5% after 20,000 cycles of test, which is overwhelming stability compared with the previously reported MXene or MXene-based materials. Fig. 8 shows the comparison of the capacity retention of the as-prepared 8 h-sonicated sample with previously reported MXene or MXene-based materials [20,29,30,31,32,33,34].

3.3. *Proposed consequence of ultrasound on synthesis of Ti_3C_2Tx MXene*

To visualize the effect of ultrasound on synthesis of accordion-like Ti_3C_2Tx MXene and compare the etching mechanism in absence of and in presence of ultrasound, a schematic was drawn and shown in Fig. 9. In the initial stage of etching, the Al atoms at the edge of Ti_3AlC_2 were removed by HF, and thereby the Ti_3AlC_2 surface was covered by the resulting AlF_3 and the Al atoms were replaced by surface terminations, such as -F, –OH, and -O, which is likely to form hydrogen bonds between two adjacent layers and impede removal of Al from the pristine Ti_3AlC_2. The as-formed AlF_3 and hydrogen bond could significantly prohibit further extraction of Al from Ti_3AlC_2 precursor and lead to low efficiency of chemical etching. In the case in presence of ultrasound, the above-mentioned AlF_3 byproducts are effectively removed from the surface of the etched Ti_3AlC_2, and more opportunities are created for the HF etchant to attack the inside Al atoms due to the acoustic cavitation effect of ultrasound. Additionally, the acoustic cavitation effect created by ultrasound can prevent/break the above-mentioned possible hydrogen bond between two adjacent layers and thereby dramatically promote the etching efficiency. Consequently, it is also reasonable to conclude that ultrasound can be also employed in other electrochemical processes, e.g., electrochemical reduction of CO_2. It was found that CO plays a unique and vital role during the electrochemical reduction of CO_2 [35], and according to our analysis, the introduction of ultrasound can boost the selectivity of CO in CO_2 electrochemical reduction, which

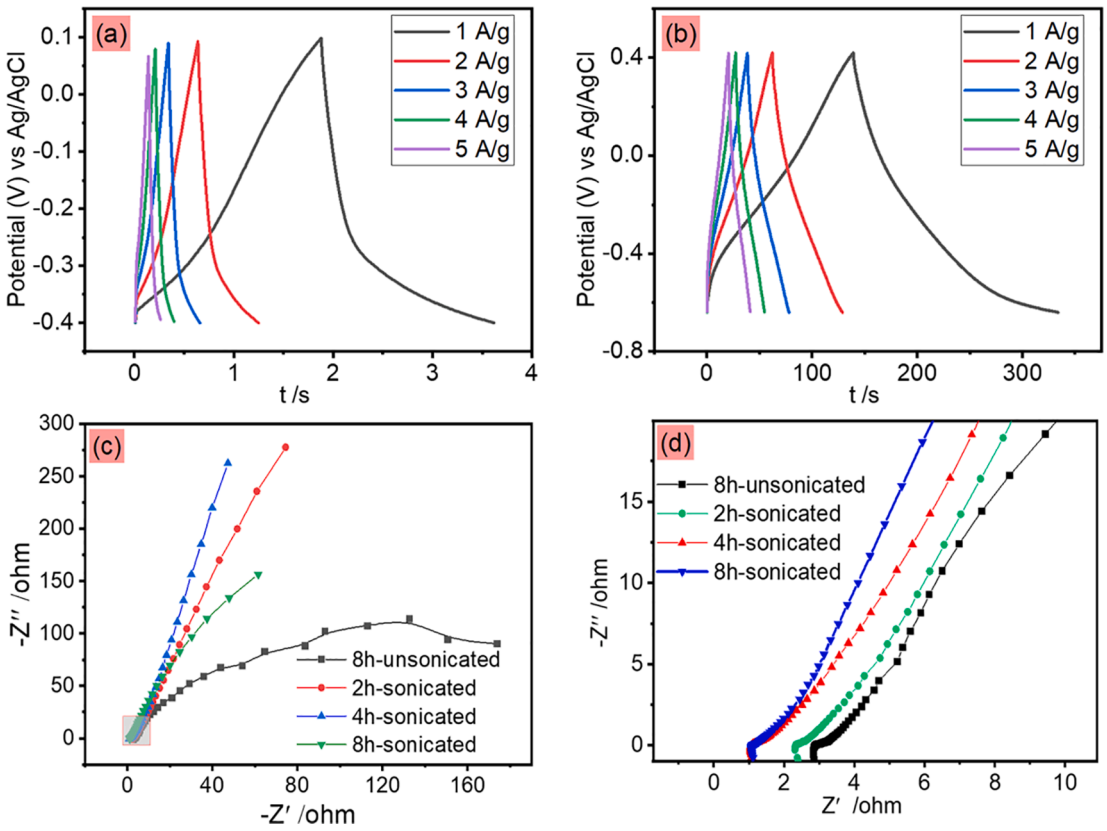

Fig. 6. GCD curves of the prepared samples with current density from 1 to 5 A/g; (a) 8 h-unsonicated; (b) 8 h-sonicated; (c) Nyquist plots of 8 h-unsonicated, 2 h-sonicated, 4 h-sonicated, and 8 h-sonicated electrodes, (d): the magnified section in the low frequency of Fig. 6(c).

Table 1
Variation of specific capacitance with different sonication time at different scan rates.

San rate (mV/s)	Specific Capacitance of the sample(F/g)			
	8 h-unsonicated	2 h-sonicated	4 h-sonicated	8 h-sonicated
10	3.4	6.9	100.2	155.0
20	3.2	6.5	85.2	138.3
40	2.9	6.2	73.9	121.7
60	2.8	5.9	66.1	110.5
80	2.8	5.5	59.4	102.4
100	2.7	5.0	48.0	89.5

is analogous to the effect of ultrasound in the present work.

4. Conclusion

In the present work, we demonstrated a highly efficient approach for the chemical etching of Ti_3AlC_2 to prepare Ti_3C_2Tx MXene with superior energy storage performance. The as-prepared Ti_3C_2Tx MXene for 8 h sonication showed a well-defined accordion-like structure, especially for the 8 h sonicated sample. XRD patterns show that the (002) planes of the etched samples shifted to a lower angle due to the broadening of the space between different layers. Furthermore, a more pronounced shift of (002) plane was observed when the ultrasound was present. SEM observation showed that well-defined accordion-like morphology is observed after 8 h treatment with ultrasound. The removal of the Al layer in the precursor was promoted significantly, only 1.63 wt% of Al is

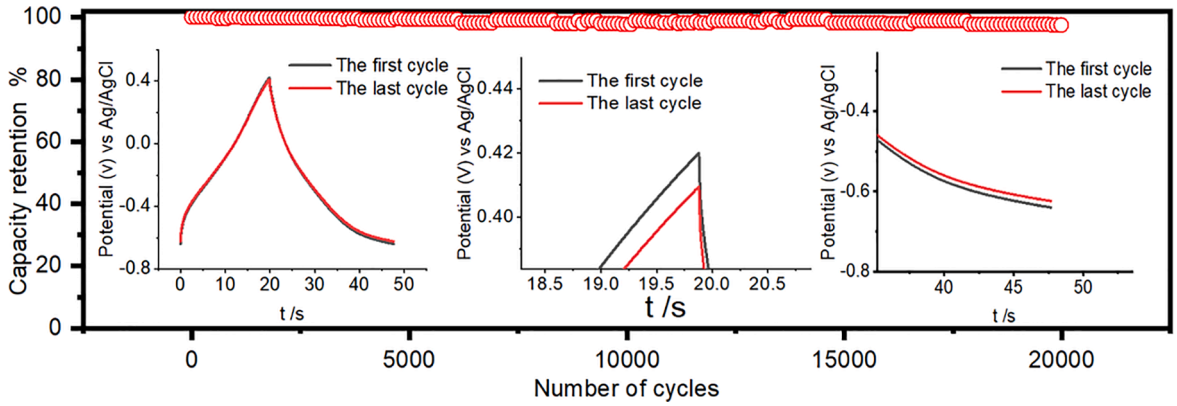

Fig. 7. Cycling stability of 8 h-sonicated sample at 5A/g; inset of Fig. 6: the GCD curves of the first cycle and the last cycle of cycling stability test.

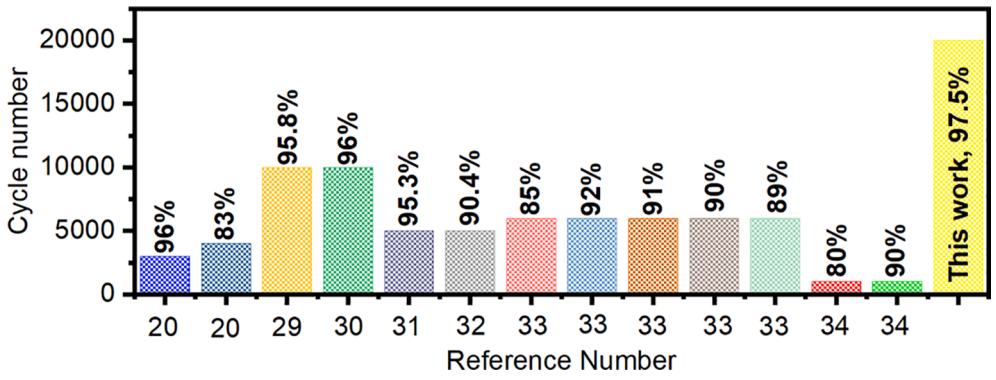

Fig. 8. Comparison of the capacity retention of the as-prepared 8 h-sonicated sample with previously reported MXene or MXene-based materials.

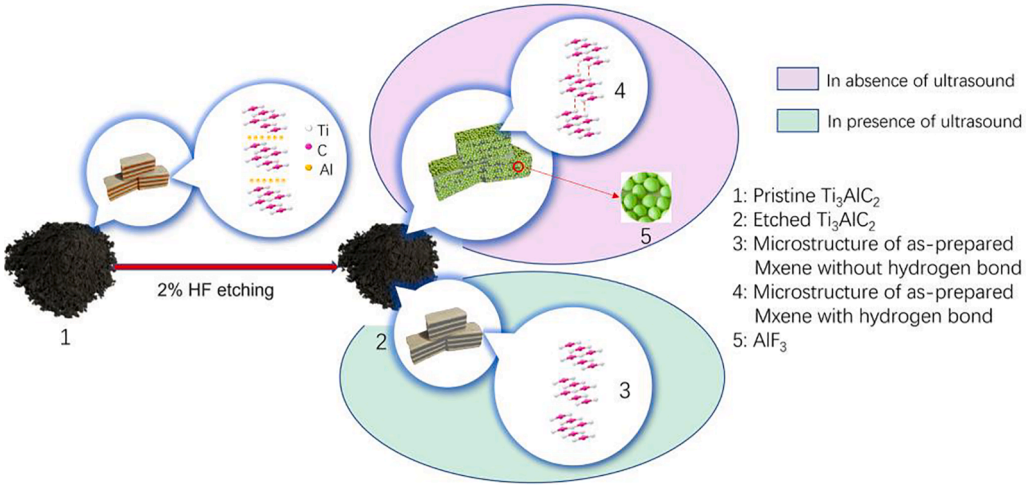

Fig. 9. Schematic of the consequence of ultrasound on the synthesis of accordion-like Ti_3C_2Tx MXene.

left in the etched sample with 8 h of sonication, while the corresponding percentage is 7.88 wt% in the counterparts without sonication. Oxidation of C and Ti in the chemical etching process was proved by XPS characterization. The specific capacitance was calculated by using CV and GCD curves, it is shown that the specific capacitance of the 8 h-sonicated sample is 155F/g, which is approximately 45-fold of the un-sonicated sample prepared with the same experimental condition. Additionally, the specific capacitance retention of the prepared 8 h sonicated sample was 97.5% after 20,000 cycles of charging/discharging, exhibiting an outstanding energy storage stability compared with the previously reported MXene or MXene-based materials.

Declaration of Competing Interest

The authors declare that they have no known competing financial interests or personal relationships that could have appeared to influence the work reported in this paper.

Acknowledgments

The authors gratefully acknowledge the financial support from the Department of Science and Technology of Liaoning Province, China (2019-ZD-0261).

References

[1] Q.-N. Zhao, Y.-J. Zhang, Z.-H. Duan, S.i. Wang, C. Liu, Y.-D. Jiang, H.-L. Tai, A review on Ti_3C_2Tx-based nanomaterials: synthesis and applications in gas and humidity sensors, Rare Metals 40 (6) (2021) 1459–1476.

[2] K. Li, T. Jiao, R. Xing, G. Zou, J. Zhou, L. Zhang, Q. Peng, Q, Peng, Fabrication of tunable hierarchical MXene@AuNPs nanocomposites constructed by self-reduction reactions with enhanced catalytic performances, Sci. China Mater. 61 (5) (2018) 728–736.

[3] X. Huang, R. Wang, T. Jiao, G. Zou, F. Zhan, J. Yin, L. Zhang, J. Zhou, Q. Peng, Facile Preparation of Hierarchical AgNP-Loaded MXene/Fe_3O_4 /Polymer Nanocomposites by Electrospinning with Enhanced Catalytic Performance for Wastewater Treatment, ACS Omega 4 (1) (2019) 1897–1906.

[4] J. Yin, F. Zhan, T. Jiao, W. Wang, G. Zhang, J. Jiao, G. Jiang, Q. Zhang, J. Gu, Q. Peng, Facile preparation of self-assembled MXene@Au@CdS nanocomposite with enhanced photocatalytic hydrogen production activity, Sci. China Mater. 63 (11) (2020) 2228–2238.

[5] N. Sheikh, M.B. Tahir, N. Fatima, M. Sagir, M. Pervaiz, M.S. Tahir, Recent advances in the rational design of 2D MXenes in energy conversion and storage systems, Int. J. Energy Res. 1–14 (2021).

[6] M. Naguib, M. Kurtoglu, V. Presser, J. Lu, J. Niu, M. Heon, L. Hultman, Y. Gogotsi, M.W. Barsoum, Two-dimensional nanocrystals produced by exfoliation of Ti_3AlC_2, Adv. Mater. 23 (37) (2011) 4248–4253.

[7] C. Zhang, X. Wang, W. Wei, X. Hu, Y. Wu, N. Lv, S. Dong, L. Shen, Recent Advances in the Synthesis and Energy Applications of 2D MXenes, ChemElectroChem. 8 (20) (2021) 3804–3826.

[8] Y.B. Li, Hui Shao, Z.F. Lin, J. Lu, L.Y. Liu, B. Duployer, P.O.A. Persson, P. Eklund, L. Hultman, M. Li, K. Chen, X.H. Zha, S.Y. Du, P. Rozier, Z.F. Chai, E. Pinero, P. Louis Taberna, P. Simon, Q. Huang, A general Lewis acidic etching route for preparing MXenes with enhanced electrochemical performance in non-aqueous electrolyte, Nature Mater. 9 (2020) 894–899.

[9] L.Y. Xiu, Z.Y. Wang, J.S. Qiu, General synthesis of MXene by green etching chemistry of fluoride-free Lewis acidic melts, Rare Metals 39 (2020) 1237–1238.

[10] C. Wen, J. Zhang, H. Zhang, C.S. Dzah, M. Zandile, Y. Duan, H. Ma, X. Luo, Advances in ultrasound assisted extraction of bioactive compounds from cash crops - A review, Ultrason Sonochem. 48 (2018) 538–549.

[11] F. Chemat, M.K.K. Zill-e-Huma, Applications of ultrasound in food technology: processing, preservation and extraction, Ultrason. Sonochem. 18 (4) (2011) 813–835.

[12] P. Sricharoen, N. Limchoowong, S. Techawongstien, S. Chanthai, Ultrasound-assisted emulsification microextraction coupled with salt-induced demulsification

based on solidified floating organic drop prior to HPLC determination of Sudan dyes in chili products, Arab. J. Chem. 12 (8) (2019) 5223–5233.
[13] J.H. Bang, K.S. Suslick, Applications of ultrasound to the synthesis of nanostructured materials, Adv. Mater. 22 (10) (2010) 1039–1059.
[14] P.R. Kumar, P.L. Suryawanshi, S.P. Gumfekar, S.H. Sonawane, Ultrasound-assisted synthesis of conducting polymer-based electrocatalysts for fuel cell applications, Chem. Eng. Process. 121 (2017) 50–56.
[15] Q. Wu, J. Ouyang, K. Xie, L. Sun, M. Wang, C. Lin, Ultrasound-assisted synthesis and visible-light-driven photocatalytic activity of Fe-incorporated TiO_2 nanotube array photocatalysts, J. Hazard. Mater. 199–200 (2012) 410–417.
[16] X. Xu, Y. Zhang, H. Sun, J. Zhou, F. Yang, H. Li, H. Chen, Y. Chen, Z. Liu, Z. Qiu, D. a. Wang, L. Ma, J. Wang, Q. Zeng, Z. Peng, Progress and perspective: MXene and MXene-based nanomaterials for high-performance energy storage devices, Adv. Electron. Mater. 7 (7) (2021) 2000967.
[17] S.Y. Lin, X. Zhang, Two-dimensional titanium carbide electrode with large mass loading for supercapacitor, J. Power Sources 294 (2015) 354–359.
[18] M. Naguib, M. Kurtoglu, V. Presser, J. Lu, J.J. Niu, M. Heon, L. Hultman, Y. Gogotsi, M.W. Barsoum, Two-Dimensional Nanocrystals Produced by Exfoliation of Ti_3AlC_2, Adv. Mater. 23 (2011) 4248–4253.
[19] W.L. Wu, D. Wei, J.F. Zhu, D.J. Niu, F. Wang, L. Wanga, L.Q. Yang, P.P. Yang, C. W. Wang, Enhanced electrochemical performances of organ-like Ti_3C_2 MXenes/polypyrrole composites as supercapacitors electrode materials, Ceram. Int. 45 (2019) 7328–7337.
[20] Y. Wei, P. Zhang, R.A. Soomro, Q.Z. Zhu, B. Xu, Advances in the synthesis of 2D MXenes, Adv. Mater. 33 (2021) 2103148–210314877.
[21] M. Alhabeb, K. Maleski, B. Anasori, P. Lelyukh, L. Clark, S. Sin, Y. Gogotsi, Guidelines for synthesis and processing of 2D titanium carbide (Ti_3C_2Tx MXene), Chem. Mater. 29 (2017) 7633–7644.
[22] O. Mashtalir, M. Naguib, B. Dyatkin, Y. Gogotsi, M.W. Barsoum, Kinetics of aluminum extraction from Ti_3AlC_2 in hydrofluoric acid, Mater. Chem. Phys. 139 (2013) 147–152.
[23] U. Gelius, P.F. Hedén, J. Hedman, B.J. Lindberg, R. Manne, R. Nordberg, C. Nordling, K. Siegbahn, Molecular Spectroscopy by Means of ESCA III. Carbon compounds, Phys. Scripta 2 (1-2) (1970) 70–80.
[24] V.D. Yumatov, G.G. Furin, A.V. Okotrub, I.A. Asanov, L.N. Mazalov, G. G. Yakobson, F Kα x-ray fluorescence spectra of fluorinated aromatic compounds, Physical Chemistry 32 (1983) 987–990.
[25] K. Li, T. Xiong, J. Liao, Y. Lei, Y. Zhang, W. Zhu, Design of MXene/graphene oxide nanocomposites with micro-wrinkle structure for efficient separating of uranium (VI) from wastewater, Chem Eng. J. 433 (2022) 134449.
[26] Z. Feng, W. Zhang, W. Liu, H. Zhang, E. Wang, Nanoporous Ni0.85Se electrocatalyst anchored on rGO for hydrazine oxidation, J. Electrochem. Soc. 168 (10) (2021) 104510.
[27] Z. Feng, E. Wang, S. Huang, J. Liu, A bifunctional nanoporous Ni-Co-Se electrocatalyst with a superaerophobic surface for water and hydrazine oxidation, Nanoscale 12 (2020) 4426.
[28] H.H. Shi, P.P. Zhang, Z.C. Liu, S.W. Park, M.R. Lohe, Y. Wu, N.A. Shaygan, S. Yang, X.L. Feng, Ambient-Stable Two-Dimensional Titanium Carbide (MXene) Enabled by Iodine Etching, Angew Chem. Int. Ed. Engl. 60 (2021) 8689–8693.
[29] S. Venkateshalu, J. Cherusseri, M. Karnan, K.S. Kumar, P. Kollu, M. Sathish, J. Thomas, S.K. Jeong, A.N. Grace, New Method for the Synthesis of 2D vanadium nitride (MXene) and its application as a supercapacitor electrode, ACS Omega. 5 (2020) 17983–17992.
[30] L.F. Li, F. Wang, J.F. Zhu, W.L. Wu, The facile synthesis of layered Ti_2C MXene/carbon nanotube composite paper with enhanced electrochemical properties, Dalton Trans 46 (2017) 14880–14887.
[31] J. Li, X. Yuan, C. Lin, Y. Yang, L.e. Xu, X. Du, J. Xie, J. Lin, J. Sun, Achieving high pseudocapacitance of 2D titanium carbide (MXene) by cation intercalation and surface modification, Adv. Energy Mater. 7 (15) (2017) 1602725.
[32] C.J. Zhao, Q. Wang, H. Zhang, S. Passerini, X.Z. Qian, Two-dimensional titanium carbide/rGO composite for high performance supercapacitors, ACS Appl. Mater. Interfaces 8 (2016) 15661–15667.
[33] H.M. Jiang, Z.G. Wang, Q. Yang, M. Hanif, Z.M. Wang, L.C. Dong, M.D. Dong, A novel MnO_2/Ti_3C_2Tx MXene nanocomposite as high-performance electrode materials for flexible supercapacitors, Electrochimi. Acta 290 (2018) 695–703.
[34] M. Ma, H.A. Hansen, M. Valenti, Z. Wang, A. Cao, M. Dong, W.A. Smith, Electrochemical Reduction of CO_2 on Compositionally Variant Au-Pt Bimetallic Thin Films, Nano Energy 42 (2017) 51–57.
[35] X.Q. Li, C.G. Wang, Y. Cao, G.X. Wang, Functional MXene materials: progress of their applications, Chem. Asian J. 13 (2018) 2742–2757.